Dielectric permittivity method to monitor (liquid) water content in unsaturated soils, frozen soils, and snow

Alessandro Tarantino[1,*], *Roberta* Dainese[2], *Carla* Pendino[3], and *Giulia* Guida[4]

[1] University of Strathclyde, Department of Civil and Environmental Engineering, Glasgow, Scotland (UK)
[2] Agenzia Regionale per la Prevenzione e Protezione Ambientale del Veneto, Centro Valanghe di Arabba Veneto, Belluno, Italy
[3] Agenzia Provinciale per la Protezione dell'Ambiente - Provincia Autonoma di Trento, Trento, Italy
[4] Università degli Studi di Roma Tor Vergata, Dipartimento di Ingegneria Civile e Ingegneria Informatica, Roma, Italy,

Abstract. Monitoring (liquid) water content is key to inform early-warning systems for unsaturated, permafrost, and snow slopes. Dielectric permittivity-based sensors are widely used to monitor (liquid) water content in unsaturated soils and include the well-known TDR and capacitive probes. In contrast to unsaturated soils, there are no established methods to measure liquid water content in frozen soils and snow. This paper introduces the 'refractive index' mixing model for four-phase materials (solids, air, liquid water, and solid water) as a unifying equation to interpret dielectric permittivity measurements in unsaturated soils, frozen soils, and snow. The mixing model is first used to revisit empirical equations used to estimate the water content in unsaturated soils. It is then validated against TDR measurements of bulk density in dry snow. Its use to monitor the liquid water content in frozen soils and snow is finally discussed.

1 Introduction

Unsaturated soils experience shear strength changes when their water content. Monitoring (liquid) water content is therefore key to inform early-warning systems for rainfall-induced landslides impacting transport networks and urban areas. Dielectric permittivity-based sensors are widely adopted to monitor (liquid) water content in unsaturated soils and include the well-known TDR and capacitive probes [[1]].

Variation in (liquid) water content is also critical in permafrost regions because the phase change from solid to liquid due to thawing often triggers landslides [[2], [3]]. Similarly, wet snow-avalanches commonly occur during the springtime triggered mainly by the melting of ice and the consequent pore-space filling with capillary liquid water [[4], [5]], i.e., the snow slope becomes susceptible to failure when 'unsaturated'. In contrast to unsaturated soils, there are no established methods to measure liquid water content in frozen soil and snow, especially with direct, non-destructive and continuous methods.

This paper unravels the Refractive Index Mixing Model (RIMM) as a unifying tool for dielectric permittivity-based measurement of liquid water content in unsaturated soils, frozen soils, and snow. It first discusses the RIMM to revisit empirical equations commonly adopted to estimate the water content in unsaturated soils (i.e., Topp and Ledieu's equations) to reveal the range of dry densities where these empirical equations can be applied. It then probes the refractive index mixing model against measurement of bulk density of dry snow to demonstrate its validity for the case where the solid phase is constituted of ice. It finally discusses the potential use of the RIMM to measure liquid water content in frozen soils and snow.

2 Water content in unsaturated, permafrost, and snow slopes

2.1 Unsaturated slopes

Rainfall-induced landslides typically occur in coarse-grained covers and are triggered by the increase in water content due to rainwater infiltration, which in turn reduces suction and shear strength. They often cause significant damage and fatalities. For these hazards, early-warning systems are the mostly adopted strategy to reduce landslide risk [[6], [7]]. Early-warning systems are based on landslide precursors rather than indicators as the rapidity of the sliding mass typically does not leave enough time to issue an alarm. Volumetric water content measured by dielectric-permittivity-based sensors has been included as additional precursor variable to inform early-warning [[8], [9]]. A reliable measurement of volumetric water content via the measurement of the soil apparent dielectric permittivity is therefore needed.

2.2 Permafrost slopes

The unfrozen water content in permafrost-affected soils plays a crucial role in determining the hydro-mechanical

---

[*] Corresponding author: alessandro.tarantino@strath.ac.uk

behaviour of slopes in cold regions. Even at several degree below 0°C, a certain amount of water remains in a liquid state due to solid-liquid interacting forces, particularly in fine-grained soils such as silts and clays [[10]]. As a result, the hydro-mechanical properties of the permafrost soils are strongly influenced by temperature variations even below the freezing point.

The amount of unfrozen water affects the soil's shear strength [[11]], permeability [[12]], and creep behaviour under long-term loading [[13]]. An increase in unfrozen water content, i.e., caused by rising temperatures, can significantly reduce the shear strength, potentially compromising the stability of permafrost slopes [[14]]. Accurate monitoring of the unfrozen water content is therefore essential to predict slope performance under changing environmental conditions, enabling a more comprehensive understanding of permafrost slope dynamics and supporting effective risk mitigation strategies in cold regions.

2.3 Snow slopes

The trigger of wet snow avalanches is related to the presence of liquid water within the snowpack, due to rising temperatures or infiltration of rain [[15]]. The mechanism of failure is still not well known, caused by the loss of strength due to water accumulation at the level of capillary barriers, overloading of partially wet snowpack, and/or weakening of the basal layer and the reaching of a total or partial isothermal condition along the snowpack [[16]].

Despite the high damage potential of wet-snow avalanches, especially during the spring period, the forecast of wet snow avalanches days is still a challenge, due, among other factors, to the difficulty in describing the effect of liquid water on snow mechanical properties and the difficulty in obtaining reliable in-situ measurements of liquid water content [[17]-[19]]. Although a good correlation with air temperature was found [[20]], it resulted to be insufficient for forecast purposes [[16], [21]], to which the assessment of liquid water content is valued to be the most important factor [[22]].

3 Refractive Index Mixing Model (RIMM)

The (real part) of the dielectric permittivity of a mixture ε_m can be expressed via the Litchteneker equation [[23]]

$$\sqrt{\varepsilon_m} = \frac{V_s}{V}(\varepsilon_s)^\alpha + \frac{V_a}{V}(\varepsilon_a)^\alpha + \frac{V_w}{V}(\varepsilon_w)^\alpha + \frac{V_{ice}}{V}(\varepsilon_{ice})^\alpha \quad (1)$$

where V_s, V_a, V_w, and V_{ice} are the volumes of the solids, air, liquid water, and ice respectively, V is the total volume of the mixture, ε_s, ε_a, ε_w, and ε_{ice} are the values of dielectric permittivity of the solids, air, liquid water, and ice respectively, and α an exponent that depends on the spatial arrangement of the mixture with the respect to the applied electromagnetic field. For a heterogeneous layered medium, the exponent varies between α=-1 for an electromagnetic field orthogonal to the layers, and α=-1 for a parallel field [[24]].

The Litchteneker model for α=0.5 is referred to as 'refractive index' mixing model (RIMM). It is associated with an isotropic distribution of the four phases and has been found to capture satisfactorily experimental data for mineral soils [[25], [26]].

The volume fractions in Eq. (1) can be expressed in terms of phase relationship as follows:

$$\begin{aligned} \frac{V_w}{V} &= \theta \\ \frac{V_{ice}}{V} &= \frac{\rho_{d,ice}}{\rho_{ice}} \\ \frac{V_s}{V} &= \frac{\rho_d}{\rho_s} \\ \frac{V_a}{V} &= 1 - \frac{\rho_d}{\rho_s} - \theta - \theta_{ice} \end{aligned} \quad (2)$$

where θ is the volumetric water content of the liquid water, ρ_d and $\rho_{d,ice}$ are the dry density of the soil and ice respectively, ρ_s and ρ_{ice} are the density of the solids and ice respectively.

By combining Eqs. (1) and (2), the calibration equation to derive the (liquid) volumetric water content θ from the dielectric permittivity ε_m of the mixture can be derived as:

$$\theta = a\sqrt{\varepsilon_m} - b \quad (3)$$

where:

$$\begin{aligned} a &= \frac{1}{\sqrt{\varepsilon_w} - \sqrt{\varepsilon_a}} \\ b &= \frac{\frac{\rho_d}{\rho_s}\sqrt{\varepsilon_s} + \frac{\rho_{d,ice}}{\rho_{ice}}\sqrt{\varepsilon_{ice}} + \left(1 - \frac{\rho_d}{\rho_s} - \frac{\rho_{d,ice}}{\rho_{ice}}\right)\sqrt{\varepsilon_a}}{\sqrt{\varepsilon_w} - \sqrt{\varepsilon_a}} \end{aligned} \quad (4)$$

Eqs. (3) and (4) provide a general calibration equation for unsaturated soils ($\rho_{d,ice}$=0), frozen soils, and snow (ρ_d=0). It is worth noticing that the intercept *b* depends on the dry density of the soil and/or ice.

4 Unsaturated soils

4.1 Refractive index mixing model versus density-independent empirical equations

To evaluate the mixing model, the case of unsaturated is first considered here and compared with two popular empirical equations widely adopted to infer the volumetric water content from the dielectric permittivity, i.e. Topp [[27]] and Ledieu [[28]] equations:

Topp's equation

$$\theta = -5.3 \cdot 10^{-2} + 2.92 \cdot 10^{-2} K_a - 5.5 \cdot 10^{-4} K_a^2 + 4.3 \cdot 10^{-6} K_a^3 \quad (5)$$

Ledieu's equation

$$\theta = 0.1138\sqrt{K_a} - 0.1758 \quad (6)$$

These two empirical equations derive the volumetric water content from the apparent dielectric permittivity

K$_a$, which can be assumed to be equal to the (real part of the) dielectric permittivity ε_m for the case of soils with negligible electrical conductivity.

Fig. 1 shows the calibration curve derived from the refractive index mixing model for two different soil dry densities (ρ_d=1.3/1.5 g/cm^3) for against the empirical equations by Topp and Ledieu (parameters considered for the mixing model in Table 1). The curves are essentially overlapping up to θ = 0.4 with slight deviation for $\theta > 0.4$.

The slope and intercept of the calibration curve, *a* and *b* respectively, are given in Table 2 where they are compared with the values of the Ledieu's empirical equation. The parameter *b* depends on the soil dry density ρ_d, and the two values considered in this exercise, 1.3 and 1.5 g/cm^3,encompass the values tested by Topp et al. [[27]] when first developing their seminal cubic empirical equation.

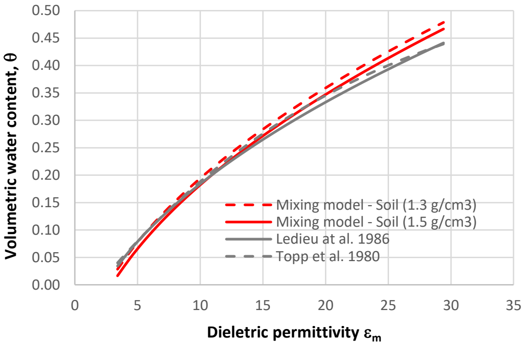

Fig. 1. Calibration curve derived from the 'refractive' mixing model compared to the empirical models by [[27], [28]]

Table 1. Values inputted in Eqs. (4) to assess the mixing model versus density-independent empirical equations

ε_s [-]	ε_a [-]	ε_w [-]	ρ_d [g/cm^3]	ρ_s [g/cm^3]
5	1	80	1.3/1.5	2.6

Table 2. Comparison between the mixing model and empirical equation by Ledieu et al. (1986).

	Mixing model (ρ_d=1.5 g/cm^3)	Mixing model (ρ_d=1.3 g/cm^3	Ledieu et al (1986)
a	0.1259	0.1259	0.1138
b	0.2156	0.2037	0.1758

4.2 Refractive index mixing model versus density-dependent empirical equations

Eq. (4) shows that the calibration equation for the liquid water content depends on the soil dry density. When the soil dry density falls outside the range investigated by Topp [[27]] and Ledieu [[28]] when developing their empirical equations, Eqs. (5) and (6) are no longer applicable.

For the case of low density (ρ_d<0.8g/cm^3) organic soils, Malicki *et al.* [[29]] have developed the following empirical equation:

$$\theta = \frac{\sqrt{Ka} - 0.819 - 0.168\rho_d - 0.159\rho_d^2}{7.17 + 1.18\rho_d} \qquad (7)$$

where the dependency of the volumetric water content, θ, on the apparent dielectric permittivity, *K*$_a$, is corrected for the dry density, ρ_d.

Fig. 2 shows the Malicki's model compared to the RIMM for the case of ρ_d=0.8 g/cm^3. For comparison, the Ledieu's equation is also shown in the figure. The lower dry density shifts the calibration curve upward, for both the RIMM and Maliki's equation. This shows once again that the traditional Ledieu's and Topp's empirical equations only apply to a relatively narrow range of dry density, typically encountered in agricultural soils. They do not hold anymore for lower dry densities as is the case of organic soils or very high dry densities as is the case of compacted soils.

It should be noted that there is a discrepancy between the Malicki's and the RIMM models. This may partly be attributed to the likely non-negligible electrical conductivity of the organic soils that makes $\varepsilon_m \neq K_a$. A discussion on the effect of the soil electrical conductivity is, however, outside the scope of this paper.

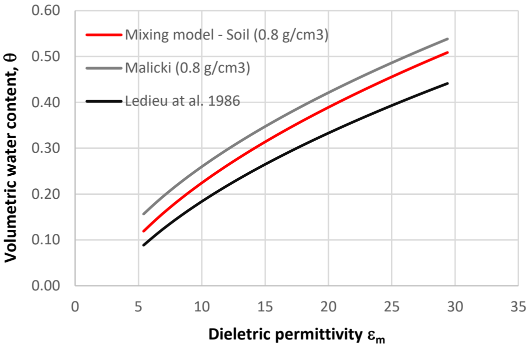

Fig. 2. Calibration curve derived from the 'refractive' mixing model compared to the empirical models by [[29]]

Table 3. Values inputted in Eqs. (4) to assess the mixing model versus density-dependent empirical equation

ε_s [-]	ε_a [-]	ε_w [-]	ρ_d [g/cm^3]	ρ_s [g/cm^3]
5	1	80	1.0/2.0	2.6

5 Probing the refractive index mixing model in 'dry' snow

5.1 Time Domain Reflectometry (TDR)

A TDR system consists of a step pulse generator, an oscilloscope, a coaxial cable and a rod probe (Fig. 3). The step pulse generator launches a fast-rise time voltage step associated with a bandwidth up to 1.5 GHz and the reflection waveform is recorded by an equivalent time sampling oscilloscope. The higher frequencies are sufficiently lower than relaxation frequency of water and fall in the range where the effect of electrical conductivity is often negligible [[1]].

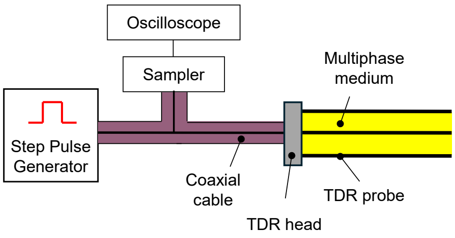

Fig. 3. TDR system

Fig. 4 shows the reflection waveforms measured in air and water. When the electromagnetic wave enters the probe, the lower impedance of the probe immersed in water compared to the coaxial cable causes an initial drop in the reflection coefficient (~49 ns). When the wave reaches the end of the probe, the wave is fully reflected, and this causes a rise of the waveform (~59 ns). Differently from water, the probe in air has higher impedance compared to the coaxial cable and this causes an increase in the reflection coefficient when the wave enters the probe (~49 ns).

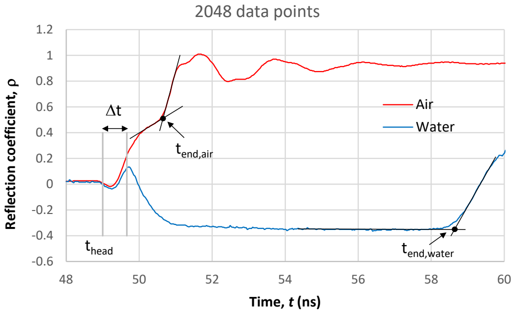

Fig. 4. Measurement in air and water to calibrate TRD probe electrical length L and the time t_{probe} at which the step pulse leaves the head and enters the probe.

The apparent dielectric permittivity K_a is determined through Eq. (8)

$$2L\frac{\sqrt{K_a}}{c} = t_{end} - t_{probe} \qquad (8)$$

where c is the speed of light in a vacuum (3×10^8 m s^{-1}), L is the electrical length of the probe (m), t_{probe} is the time at which the wave enters the probe and t_{end} is the time at which the wave is reflected at the end of the probe.

The time t_{end} corresponding to the reflection at the end of the probes can be determined by considering the intersection between the line tangent to the second rising limb at the inflection point and the line fitting the base section of the reflection waveform (Fig. 4).

The time at which the wave enters the probe, t_{probe}, is not easily detected because probes commercially available incorporates an electrical marker causing a dip in the reflected waveform whet the wave passes through the head. The time t_{probe} can effectively be determined by calibrating the probe in air and water.

We can write

$$t_{probe} = t_{head} + \Delta t \qquad (9)$$

where t_{head} is the time at which the wave enters the probe and Δt is the travel time through the probe. If Eqs. (8) and (9) are written for air and water ($K_{a,air}$=1 and $K_{a,water}$=80.2 at 20°C) the two unknowns Δt and L can be determined as follows:

$$\Delta t = \frac{\frac{\sqrt{K_a}}{\sqrt{K_w}}\left(t_{end,w} - t_{head}\right) - \left(t_{end,a} - t_{head}\right)}{\frac{\sqrt{K_a}}{\sqrt{K_w}} - 1} \qquad (10)$$

$$L = \frac{1}{2}\frac{c}{\sqrt{K_{air}}}\left[t_{end,a} - \left(t_{head} + \Delta t\right)\right]$$

The time t_{probe} can therefore be obtained by via Eq. (9).

5.2 TDR measurements in 'dry' snow

Snow was collected along the trunk road S.S. 350 close to Passo del Sommo, located near Folgaria in the province of Trento in Italy. The snow was stored in a freezer and then compacted in moulds 20 cm high and 10 cm diameter at different densities ($\rho_{d,ice}$=0.363, 0.417, 0.444, 0.467, 0.536, 0.598 g/cm^3). Following compaction, the TDR probe was inserted in the snow specimen (Fig. 5) and the TDR measurement was taken with the specimen remaining in the freezer.

Fig. 5. TDR probe in snow-filled mould

The waveforms recorded for two values of bulk density are shown in Fig. 6, where the waveform in air is also shown for comparison. The increasing dry density shifts the waveform towards the right-hand side because the dielectric permittivity of the mixture increases due to the higher fraction of solid water (ice). The apparent permittivity K_a was then determined from the waveforms by detecting t_{end} as shown in Fig. 6 and using Eq. (8).

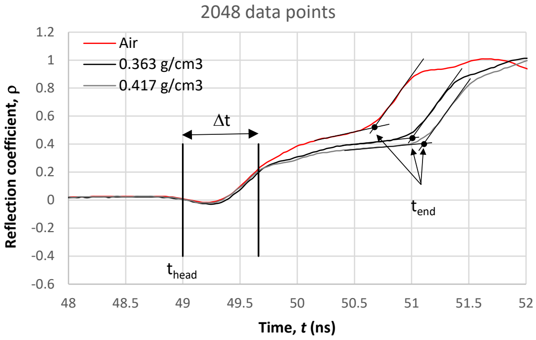

Fig. 6. Reflection waveforms in dry snow at low dry densities

The relationship between dry density and dielectric permittivity was then determined theoretically using the refractive index mixing model defined by Eqs. (1) and (2) and considering θ=0, ρ_d=0, and ε_m=K_a. The theoretical relationship (parameters in Table 4) is shown in Fig. 7 together with the experimental data. There is an excellent agreement between experimental data and the mixing model, which demonstrates its robustness.

Table 4. Values inputted in Eqs. (4) to derive the dielectric permittivity for dry snow via the mixing model

ε_s [-]	ε_a [-]	ρ_{ice} [g/cm^3]
3	1	0.9

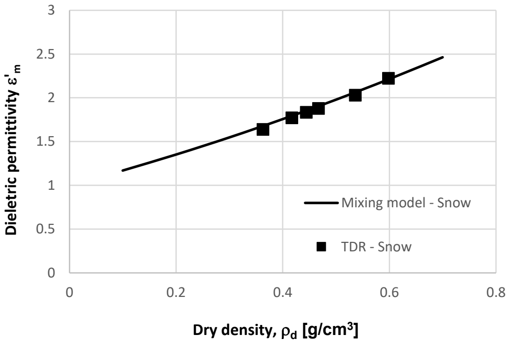

Fig. 7. Dielectric permittivity versus dry density: mixing model versus experimental data

6 Using the RIMM for measurements of (liquid) water content in snow and frozen soils

Let us consider the snow to be initially dry and characterised by an ice dry density $\rho_{d,ice0}$:

$$\rho_{d,ice0} = \frac{M_{ice0}}{V} \tag{11}$$

where M_{ice0} is the initial mass of ice in dry snow and V is the total volume. The density of the dry snow can be measured using the calibration curve in Fig. 7, possibly taking the measurement overnight when the temperature typically drops below zero.

The formation of liquid water occurs at the expenses of the melting of ice. Because the mass of species 'water' remains constant, we can write:

$$M_{ice0} = M_{ice} + M_l \tag{12}$$

where M_{ice} and M_l are the masses of ice and liquid water respectively after melting. Moreover, the mass of liquid water can be expressed as:

$$M_l = \theta\, V \rho_l \tag{13}$$

where ρ_l is the density of liquid water. By replacing Eqs. (11), (12), (13), and (2) in Eq. (1) and assuming $\rho_l \cong \rho_{ice}$, one can derive:

$$\begin{aligned} a &= \frac{1}{\left(\frac{\rho_l}{\rho_{ice}} - 1\right)\sqrt{\varepsilon_a} + \sqrt{\varepsilon_l} - \frac{\rho_l}{\rho_{ice}}\sqrt{\varepsilon_{ice}}}\sqrt{\varepsilon_m} \\ b &= \frac{\left(\frac{\rho_{d,ice0}}{\rho_{ice}}\sqrt{\varepsilon_{ice}} + \sqrt{\varepsilon_a} - \frac{\rho_{d,ice0}}{\rho_{ice}}\sqrt{\varepsilon_a}\right)}{\left(\frac{\rho_l}{\rho_{ice}} - 1\right)\sqrt{\varepsilon_a} + \sqrt{\varepsilon_l} - \frac{\rho_l}{\rho_{ice}}\sqrt{\varepsilon_{ice}}} \end{aligned} \tag{14}$$

As an example, Fig. 8 shows the calibration curve for snow at ice dry density of $\rho_{d,ice0}$=0.25 g/cm^3. The same figure shows the calibration curve for 'mineral' soils for comparison.

Same considerations can be made for frozen soils. However, a frozen soil is a four-phase system as opposed to snow (including soil, ice, air, and liquid water) and an independent determination of the soil dry density is required. This is the reason why approaches for the determination of liquid water content in frozen soils couples two independent measurement techniques, for example TDR and gamma ray attenuation [[30]];

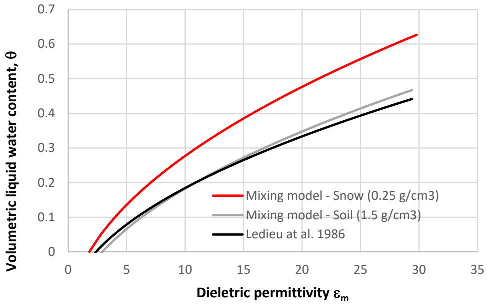

Fig. 8. Dielectric permittivity versus dry density: mixing model versus experimental data

7 Conclusions

This paper has introduced the Refractive Index Mixing Model (RIMM) for four-phase materials (solids, air, liquid water, and solid water) as a unifying equation to interpret dielectric permittivity measurements in unsaturated soils, frozen soils, and snow. The mixing model was first used to revisit empirical equations used to estimate the water content in unsaturated soils from the measurement of the soil dielectric permittivity. It was shown that the traditional Topp's and Ledieu's empirical equation are captured by the RIMM of developed using the same range of dry density of the samples that formed the database used to develop the Topp's and Ledieu's empirical equation. At the same time, lower or higher dry densities make the Topp's and Ledieu's empirical equations no longer applicable with the RIMM providing a possible alternative.

The RIMM was then validated against TDR measurements of bulk density of dry snow. Its use to monitor the liquid water content in frozen soils and snow was finally discussed, for further investigation with bespoke experimental programmes.

References

[1]. A. Tarantino, A. Ridley, D. Toll, Field Measurement of Suction, Water Content, and Water Permeability. Geotech. Geol. Eng. **26**, 751-782 (2008). DOI: 10.1007/s10706-008-9205-4.

[2]. F. Niu, J. Luo, Z. Lin, et al., Thaw-induced slope failures and stability analyses in permafrost regions of the Qinghai-Tibet Plateau, China. Landslides **13**, 55–65 (2016). https://doi.org/10.1007/s10346-014-0545-2

[3]. S. Subramanian, T. Ishikawa, T. Tokoro, Stability assessment approach for soil slopes in seasonal cold regions. Eng. Geol. **221**, 154-169 (2017). https://doi.org/10.1016/j.enggeo.2017.03.008.

[4]. D. McClung, P.A. Schaerer, The avalanche handbook, (The Mountaineers Books, 2006)

[5]. M. Schneebeli M, Mechanisms in wet snow avalanche release, in Proceedings ISSMA-2004, International symposium on snow monitoring and avalanches, Snow and Avalanche Study Establishment, Manali, India, 12–16 April (2004), 75–77

[6]. L. Alfieri, P. Salamon, F. Pappenberger, F. Wetterhall, J. Thielen, Operational early warning systems for water-related hazards in Europe. Environmental Science & Policy **21**: 35–49 (2012). http://dx.doi.org/10.1016/j.envsci.2012.01.008,

[7]. R. Greco, L. Pagano, Basic features of the predictive tools of early warning systems for water-related natural hazards: examples for shallow landslides. Natural Hazards Earth System Sciences **17**: 2213-2227 (2017). https://doi.org/10.5194/nhess-17-2213-2017, 2017

[8]. S. Segoni, A. Rosi, D. Lagomarsino, R. Fanti, N. Casagli, Brief communication: Using averaged soil moisture estimates to improve the performances of a regional-scale landslide early warning system. Nat. Hazards Earth Syst. Sci. **18**: 807–812 (2018). https://doi.org/10.5194/nhess-18-807-2018

[9]. B. Thiebes, R. Bell, T. Glade, S. Jäger, J. Mayer, M. Anderson, L. Holcombe, Integration of a limit-equilibrium model into a landslide early warning system. Landslides **11**: 859–875 (2014). https://doi.org/10.1007/s10346-013-0416-2

[10]. P.J. Williams, Unfrozen water content of frozen soils and soil moisture suction. Geotechnique, **14**(3): 231-246 (1964).

[11]. F. Casini, A. Gens, S. Olivella, G.M. Viggiani Artificial ground freezing of a volcanic ash: laboratory tests and modelling. Environmental Geotechnics, **3**(3): 141-154 (2014)

[12]. F. Ming, M. Zhang, W. Mei, L. Chen, A new hydraulic conductivity model of frozen soil considering the hysteresis effect based on fractal theory. Geoderma, **442**: 116790 (2024).

[13]. U. Schindler, R. Cudmani, S. Chrisopoulos, A. Schünemann, Multi-stage creep behavior of frozen granular soils: experimental evidence and constitutive modeling. Canadian Geotechnical Journal, **61**(1): 118-133 (2023).

[14]. F. Niu, G. Cheng, W. Ni, D. Jin, Engineering-related slope failure in permafrost regions of the Qinghai-Tibet Plateau, Cold Regions Science and Technology, **42**(3): 215-225 (2005).

[15]. R. Armstrong, Wet snow avalanches, in Armstrong, R., Ives, J. (Eds.), Avalanche Research and Snow Characteristics, San Juan Mountains, Colorado, University of Colorado INSTAAR (1976), 67–82

[16]. S. Baggi, J. Schweizer, Characteristics of wet-snow avalanche activity: 20 years of observations from a high alpine valley (Dischma,Switzerland). Natural Hazards **50**: 97-108 (2009).

[17]. K. Izumi, E. Akitaya, Hardness of wet snow. Ann. Glaciol. **6**: 267–268 (1985)

[18]. F. Techel, C. Pielmeier, M. Schneebeli, Microstructural resistance of snow following first wetting. Cold Regions Science and Technology **65**(3): 382-391 (2011):

[19]. L. Schmid, F. Koch, A. Heilig, M. Prasch, O. Eisen, W. Mauser, J. Schweizer, A novel sensor combination (upGPR-GPS) to continuously and nondestructively derive snow cover properties. Geophysical Research Letters **42**(9): 3397-3405 (2015).

[20]. E. H. Peitzsch, G.T. Pederson, K.W. Birkeland, J. Hendrikx, D.B. Fagre, Climate drivers of large magnitude snow avalanche years in the US northern Rocky Mountains. Scientific Reports **11**(1): 1–13 (2021)

[21]. J.M. Romig, S. Cluster , K. Birkeland, W. Locke, March wet avalanche prediction at Bridger Bowl ski area, Montana, in Elder, K. (ed.), Proceedings ISSW 2004, International Snow Science Workshop, Jackson Hole WY, U.S.A., 19-24 September 2004, 598–607 (2005)

[22]. M. Hendrick, F. Techel, M. Volpi, T. Olevski, C. Pérez-Guillén, A. Herwijnen, J. Schweizer, Automated prediction of wet-snow avalanche activity in the Swiss Alps. Journal of Glaciology **69**(277): 1365–1378 (2023). https://doi.org/10.1017/jog.2023.24

[23]. K. Lichtenecker K. Die dielektrizitatskonstante naturlicherund kunstlicher mischkorper. Physikalische Zeitschrift, **27**:115–158 (1926)

[24]. T. Zakri, J.P. Laurent, M. Vauclin. Theoretical evidence of the Lichtenecker's mixture formulae based on the effective medium theory. J. Phys. D Appl. Phys. 31: 1589–1594 (1998).

[25]. D.A. Robinson, C.M.K. Gardner, J.D. Cooper Measurement of relative permittivity in sandy soils using TDR, capacitance and theta probes: comparison, including the effects of bulk soil electrical conductivity. J. Hydrol. **223**: 198–211 (1999)

[26]. K. Roth, R. Schulin, H. Flühler, W. Attinger, Calibration of TDR for water content measurement using a composite dielectric approach. Water Res. Res. **26** (10): 2267-2273 (1990)

[27]. G.C. Topp, J.L. Davis, A.P. Annan, Electromagnetic determination of soil water

content: Measurements in coaxial transmission lines. Water Resour. Res. **16**, 574–582 (1980)

[28]. J. Ledieu, P. De Ridder, P. De Clerck, S. Dautrebande, A method of measuring soil moisture by time domain reflectometry. J. Hydrol. **88**, 319-328 (1986)

[29]. M.A. Malicki, R. Plagge, C.H. Roth, Improving the calibration of dielectric TDR soil moisture determination taking into account the solid soil. Eur. J. Soil Sci. **47**, 357-366(1996)

[30]. X. Zhou, J. Zhou, W. Kinzelbach, F. Stauffer, Simultaneous measurement of unfrozen water content and ice content in frozen soil using gamma ray attenuation and TDR. Water Resour. Res. **50**, 9630–9655 (2014). DOI:10.1002/2014WR015640.